Identification of a small molecule that compromises the structural integrity of viroplasms and rotavirus double-layered particles

Catherine Eichwald[a], Giuditta De Lorenzo[b*], Elisabeth M. Schraner[a], Guido Papa[b], Michela Bollati[c], Paolo Swuec[d], Matteo de Rosa[c], Mario Milani[c], Eloise Mastrangelo[c], Mathias Ackermann[a], Oscar R. Burrone[b], and Francesca Arnoldi[b,e]#

Institute of Virology, University of Zürich, Zürich, Switzerland[a]; International Centre for Genetic Engineering and Biotechnology (ICGEB), Trieste, Italy[b]; Biophysics Institute of the National Research Council (CNR-IBF), Department of Biosciences, University of Milan, Milan, Italy[c]; Pediatric Clinical Research Center Fondazione Romeo ed Enrica Invernizzi, Department of Biosciences, University of Milan, Milan, Italy[d]; Department of Medicine, Surgery and Health Sciences, University of Trieste, Trieste, Italy[e]

Running Head**:** A chemical inhibitor of rotavirus replication

Address correspondence to Francesca Arnoldi, farnoldi@units.it

*Present address: Giuditta De Lorenzo, MRC – University of Glasgow Centre for Virus Research, Glasgow, UK

Word counts for abstract and text are 234 and 6,080, respectively

ABSTRACT

Despite the availability of two attenuated vaccines, rotavirus (RV) gastroenteritis remains an important cause of mortality among children in developing countries causing about 215,000 infant deaths annually. Currently, there are no specific antiviral therapies available. RV is a non-enveloped virus with a segmented double-stranded RNA genome. Viral genome replication and assembly of transcriptionally active double-layered particles (DLPs) take place in cytoplasmic viral structures called viroplasms. In this study, we describe strong impairment of the early stages of RV replication induced by a small molecule known as RNA polymerase III inhibitor, ML-60218 (ML). This compound was found to disrupt already assembled viroplasms and hamper the formation of new ones without the need of *de novo* transcription of cellular RNAs. This phenotype correlated with reduction in accumulated viral proteins and newly made viral genome segments, disappearance of the hyperphosphorylated isoforms of the viroplasm-resident protein NSP5 and inhibition of infectious progeny virus production. In *in vitro* transcription assays with purified DLPs, ML showed a dose-dependent inhibitory activity indicating the viral nature of its target. ML was found to interfere with the formation of higher order structures of VP6, the protein forming the DLP outer layer, without compromising its ability to trimerize. Electron microscopy of ML-treated DLPs showed a dose-dependent structural damage. Our data suggest that interactions between VP6 trimers are essential not only for DLP stability but also for the structural integrity of viroplasms in infected cells.

IMPORTANCE

Rotavirus gastroenteritis is responsible for a large number of infant deaths in developing countries. Unfortunately, in those countries where effective vaccines are urgently

needed, the efficacy of the available vaccines is particularly low. Therefore, the development of antivirals is an important goal, as they might complement the available vaccines or represent an alternative option. Moreover, they may be decisive in fighting the acute phase of infection. This work describes the inhibitory effect on rotavirus replication of a small molecule initially reported as an RNA polymerase III inhibitor. The molecule is the first chemical compound identified able to disrupt viroplasms, the viral replication machinery, and to compromise the stability of DLPs by targeting the viral protein VP6. This molecule thus represents a starting point towards the development of more potent and less cytotoxic compounds against rotavirus infection.

INTRODUCTION

Rotavirus (RV) is the most common cause of gastroenteritis in young children and infants throughout the world. The impact of RV vaccines on global estimates of RV mortality has been limited, and the rate of deaths due to RV gastroenteritis in developing countries is still approximately between 197,000–233,000 per year (1). Currently, there are no specific antivirals available. The virus belongs to the *Reoviridae* family, is non-enveloped and contains a genome of eleven segments of double-stranded RNA. During entry into the host cell (enterocytes of the intestinal villi), the virion (triple-layered particle, TLP) loses the outer of its three concentric protein layers formed by the glycoprotein VP7 and the spike protein VP4 and becomes a transcriptionally active double-layered particle (DLP). The viral RNA-dependent RNA polymerase VP1 acts both as transcriptase (synthesis of viral mRNAs) and as replicase (synthesis of minus strands resulting in new genome segments) (2). To be transcriptionally active, VP1 must be localized within a DLP. Both DLP layers, the inner one formed by VP2 and the outer one formed by VP6 trimers, are required to guarantee transcriptional activity.

Removal of VP6 from DLPs abolishes this activity, which can be recovered by adding native or recombinant VP6 (3, 4). The transcribed plus-stranded RNAs act as both messengers for viral protein synthesis and templates for viral genome replication. The viral genome is replicated in viral cytoplasmic structures called viroplasms, where also the assembly of progeny DLPs takes place. These newly synthesized DLPs perform a second round of transcription, called secondary transcription, which produces additional plus-stranded RNAs (5, 6). In the final stages of virus morphogenesis, the progeny DLPs bud into the ER acquiring a transient envelope, which is then replaced by the viral proteins (VP7, VP4) forming the outer layer of progeny TLPs (2).

In addition to the structural proteins forming DLPs (VP1, the capping enzyme VP3, VP2, and VP6), two viral non-structural proteins are also found in viroplasms: NSP5 and NSP2. Both are essential for viroplasm formation and therefore for viral replication (6-9). During viral infection, NSP5 undergoes a complex hyperphosphorylation process involving different kinases and interactions with other viral proteins (10-12). However, the role of this post-translational modification in the viral replication cycle is not completely understood. In fact, several lines of evidence show correlation between viroplasm formation and NSP5 phosphorylation (13-15). Also, NSP2 and VP2 were recently found phosphorylated, and it has been proposed that viroplasm formation is a phosphorylation-dependent process (11).

The number and size of viroplasms in infected cells are indicative of viral replication efficiency. These values decrease in the presence of compounds with antiviral effect on the early steps of the viral cycle, like inhibitors of proteasome (16), microtubules (MT) (17), Eg5 kinesin (17) and thiazolides (18), that interfere with viroplasm assembly and virus infectivity. Ribavirin has also been reported to affect RV replication (19). In this work, we describe the unexpected antiviral activity of a chemical compound, ML-60218 (referred to as ML), reported

as an inhibitor of the RNA polymerase III complex (20). The effect on RV shown here is independent of the RNA polymerase III catalytic activity. For the first time, we describe a chemical compound able to disrupt viroplasms in virus-infected cells and compromise the stability of purified DLPs by interfering with interactions between VP6 trimers.

RESULTS

ML impairs viroplasm formation and disrupts already assembled viroplasms. Treatment of RV-infected cells with ML at 10 μM caused a strong reduction of viroplasms accumulated during viral replication and, in the case of the porcine OSU strain, a complete disappearance of those structures, as observed by both immunofluorescence (Fig. 1) and electron microscopy analysis (Fig. 2). Independently of whether the compound was added at 1, 3 or 5 hours post-infection (hpi), a 4 h treatment had the same effect on viroplasms (Fig. 1A). Viroplasm disruption correlated with a decrease of accumulated viral proteins, as observed with the porcine OSU and the simian SA11 strains (Fig. 1B). When added before infection, together with the infectious virion, or at 1 hpi (Fig. 1C, upper panel), ML caused a reduction of viral proteins in a dose-dependent manner with a concomitant disappearance of the NSP5 hyperphosphorylated isoforms (Fig. 1C, middle panel). ML added at the concentration of 10 μM together with the infectious virions completely blocked assembly of viroplasms (Fig. 1C, bottom panel). The same phenotype was observed in two different cell lines (monkey kidney epithelial MA104 cells and human osteosarcoma U2OS cells) upon infection with two different RV strains (OSU and SA11) (Fig. 1D and E).

The absence of viroplasms and the reduction of accumulated viral proteins indicate that ML inhibits RV replication. This result was confirmed assessing the yield of infectious progeny virus produced at different time points post-infection (Fig. 1F) and the production of

120 newly made dsRNA genome segments (gs) (Fig. 1G). During the time intervals of the
121 analysis, ML was not cytotoxic (Fig. 1H).

122 Three hours was the minimum time and 10 μM the minimal concentration required for
123 complete effect on viroplasms (data not shown). Concentrations higher than 20 μM were toxic
124 for cells, as shown by the decreased levels of actin in Western blots (Fig. 1C). Treatments of
125 up to 12-14 h at 10 μM were well tolerated (Fig. 1H).

126 **ML-mediated viroplasm disruption causes NSP5 dephosphorylation**. In order to
127 determine whether the effect of ML on NSP5 phosphorylation was due to activation of
128 phosphatases, 0.5 μM okadaic acid (an inhibitor of serine/threonine phosphatases) was
129 added to OSU-infected cells at 3 hpi (1 h before the addition of ML), and maintained during
130 the following 4 h treatment (see scheme in Fig. 3). Upon inhibition of phosphatases with
131 okadaic acid, the effect of ML on viroplasms remained unaltered (Fig. 3, bottom right panel)
132 but NSP5 hyperphosphorylated isoforms did not disappear (Fig. 3, lane 2). This result
133 suggests that the effect of ML on viroplasms is not mediated by activation of phosphatases
134 and that NSP5 dephosphorylation is the consequence of disruption of viroplasms which, when
135 intact, protect NSP5 from cytosolic phosphatases.

136 **ML activity against RV does not require newly synthesized cellular transcripts or**
137 **proteins and is independent of the RNA polymerase III catalytic activity.** To determine
138 whether the phenotype observed under ML treatment was due to *de novo* synthesis of cellular
139 proteins or RNAs, actinomycin D was added to cells at 3 h post-infection, one hour before
140 treatment with the drug, and maintained during the following 4 h treatment (see scheme in
141 Fig. 4A). Actinomycin D is a DNA intercalator that inhibits transcription of RNA polymerase I
142 at very low concentrations (>0.01 μg/ml), of RNA polymerase II at concentrations higher than
143 2 μg/ml, and of RNA polymerase III at concentrations higher than 5 μg/ml (21, 22). Newly

144 synthesized RNAs were labeled with the ribonucleoside homolog 5-ethynyl uridine (EU) and
145 visualized by reacting with an Alexa-488 conjugated azide (green) (Fig. 4A, right panel) to
146 assess the effectiveness of actinomycin D treatment. Actinomycin D at 10 µg/ml did not
147 interfere with the effect of ML indicating that newly synthesized cellular transcripts are not
148 required for ML antiviral activity. Also, in the absence of ML, treatment with actinomycin D did
149 not compromise viroplasm integrity nor affected the accumulation of viral proteins (Fig. 4A,
150 left panel). On the contrary, it slightly increased the amounts of VP2 and NSP5 compared to
151 the untreated control (Fig. 4A, lane 2 vs. lane 1). This result explains why actinomycin D was
152 found to compensate the decrease of VP2 induced by ML (Fig. 4A, left panel, lane 4 vs. lane
153 3). All these data indicate that RV replication does not require the catalytic activity of RNA
154 polymerase III and that ML activity against RV is not mediated by inhibition of this cellular
155 target. In addition, *de novo* protein synthesis is not required for ML activity. Addition of ML (at
156 4 hpi) to cells treated with the protein synthesis inhibitor cycloheximide (CHX) (added at 3 hpi)
157 still caused viroplasm disruption and NSP5 dephosphorylation (Fig. 4B).
158 **ML compromises DLPs stability.** We then investigated whether ML acts on a viral target.
159 RV DLPs were purified from cells infected with OSU or SA11 strains, and their transcriptional
160 activity tested *in vitro* in the presence of increasing ML concentrations. An irrelevant small
161 molecule (compound #7749832, ChemBridge Corp.) solubilized in the same buffer was used
162 as a control. Upon incubation with ML, the number of transcripts produced by DLPs of both
163 strains was significantly decreased in a dose-dependent manner (Fig. 5A) as compared to the
164 vehicle or the irrelevant small molecule. An IC_{50} of 10 µM was observed for both viruses. In
165 order to be transcriptionally active, DLPs must be intact. The sole absence of the external
166 layer formed by VP6 trimers is sufficient to compromise the transcriptional activity (3, 4, 21).
167 Interestingly, electron microscopy (EM) analyses on purified DLPs showed that 4 h incubation

with ML (in the same buffer used for the *in vitro* transcription assays) caused structural damage in a dose-dependent manner. DLPs with an irregular shape and partially open were observed (Fig. 5B). Quantifications in all samples are plotted in Fig. 5C. Altogether these results suggest that ML compromises the structural integrity of DLPs, thus impairing their transcriptional activity.

ML interferes with higher order VP6 structures. Although ML clearly altered DLP morphology, the EM images showed the presence of residual structures (Fig. 5, white arrows). These structures could be DLPs partially or totally deprived of the VP6 layer.

We thus investigated whether ML impaired the interaction of VP6 with VP2 or with itself, as in the formation of trimers or in the interactions between trimers.

The VP6-VP2 interaction was tested by co-immunoprecipitation with an anti-VP6 monoclonal antibody (clone RV-138) from cells overexpressing both VP6 and VP2 and treated for 5 h with ML. The inhibitor was also maintained during cell lysis and incubation with the precipitating antibody. The experiment, repeated at various ML concentrations (up to the highest concentration used of 200 μM), showed that ML did not interfere with VP6-VP2 interactions (Fig. 6A).

VP6 trimer formation was assessed by Western blots of non-boiled lysates from cells overexpressing VP6 and treated with ML. In fact, VP6 trimers (MW = 135 kDa) resist SDS denaturing and reducing conditions but not high temperatures (23). Cells infected with a recombinant vaccinia virus expressing VP6 (vvVP6) were treated with ML at 1 hpi for 7 h. VP6 trimers formed *in vivo* were not affected by the presence of ML (Fig. 6B, left panel), which did not compromise the total levels of VP6 expression. Intact VP6 trimers were also found in RV-infected cells treated with ML, although in decreased amounts because of the reduced viral replication (Fig. 6B, right panel). ML, however, appears to interfere with the

192 formation of VP6 higher order structures typically observed in cells overexpressing VP6 in the
193 absence of other RV proteins (24) (Fig. 6C). In immunofluorescence, VP6 staining showed
194 tubular structures or aggregates, while in the presence of ML it showed homogenous
195 distribution (Fig. 6C). In contrast, other structures such as viroplasm-like structures (VLS)
196 generated by overexpression of NSP5 with NSP2 (VLS-NSP2i) or with VP2 (VLS-VP2i) (24,
197 25) or with both, were not affected by ML treatment (Fig. 7A, C). Under these conditions,
198 NSP5 remained hyperphosphorylated and VP6 recruitment into VLS was not compromised
199 (Fig. 7B-C).

200 Depending on pH and ionic strength, purified VP6 self-assembles into helical tubes or
201 spherical particles ((26) and Fig. 6D, left panels). Two different types of tubes can be
202 reconstituted *in vitro*, characterized by a constant diameter of either 45 or 75 nm with a non-
203 fixed length of several µm. On the other hand, VP6 spheres are heterogeneous in size with
204 diameters varying from 75 to 100 nm (26, 27). In order to evaluate whether ML had an effect
205 on the assembly of these VP6 structures, we performed a negative staining electron
206 microscopy analysis on purified VP6 in the presence or absence of ML. Upon incubation with
207 25 µM ML, both VP6 tubes (pH 6.0) and spherical particles (pH 4.0) were severely damaged
208 (Fig. 6D). In fact, a thorough visual inspection of the EM grids failed to reveal any intact tube
209 or sphere in the presence of ML (Fig. 6D, right panels). Thus, ML has a direct effect on the
210 higher order interactions of VP6 trimers.

211 To further study the effect of ML on VP6, the interaction between the protein and the
212 drug was evaluated in nanoscale thermophoresis assays. Upon addition of the inhibitor, a
213 concentration-dependent quenching of the labeled protein was observed, which allowed us to
214 calculate an EC_{50} value of 294 ± 62 µM (Fig. 6E). Since millimolar concentrations of divalent
215 cations are known to destabilize the VP6 higher order structures shifting the equilibrium

toward isolated trimers (26), thermophoresis mobility was also tested in the presence of $CaCl_2$ (up to 500 mM). No significant changes were observed (data not shown). Thus, in the thermophoresis experimental conditions, the signal observed was due to direct binding of ML to VP6 trimers, rather than to a destabilization of its oligomerization state. Altogether, these results suggest that, although ML binds VP6 trimers with moderate affinity, it likely prevents the optimal packing of its higher oligomeric structures on the DLP outer layer. Whether this is due to a conformational change induced by the molecule or to a steric hindrance effect is not known and awaits structural confirmation.

The effect of ML on viroplasms and VP6 strongly indicates that VP6 plays an essential role in the structural integrity of viroplasms. In fact, as already reported (5), silencing VP6 expression with a specific siRNA led to a significant reduction of viroplasm number in RV-infected cells (Fig. 8A), strengthening the hypothesis that VP6 is essential for maintaining the structure of viroplasms. Of note, in ML-treated virus-infected cells VP6 was found diffused throughout the cytosol (Fig. 8B).

DISCUSSION

We describe for the first time a compound able to disrupt already formed RV viroplasms in infected cells, thus impairing RV replication as demonstrated by the decrease in viral protein translation, *de novo* synthesis of viral genomic dsRNA and yield of progeny virus. This effect of ML on RV replication was initially surprising because this drug, a cell-permeating indazole-sulfonamide small molecule, has been described to favor replication of some DNA viruses and bacteria by inhibiting the RNA polymerase III-mediated mechanism that activates the RIG-I pathway (28-30). RV, however, is an RNA virus. We ruled out that ML inhibition was mediated by RNA polymerase III activity as actinomycin D, used at a

concentration that inhibits RNA polymerase III transcription, still allowed RV replication. In addition, actinomycin D was unable to counteract the ML antiviral effect, indicating that ML antiviral activity does not require synthesis of newly made cellular transcripts, including those of RNA polymerase III. This is consistent with the finding that the ML target is of viral nature. We showed that ML impaired DLP stability *in vitro* by inhibiting the interactions between VP6 trimers. In the absence of a correctly assembled VP6 layer, DLPs lose the capacity to transcribe plus-stranded RNAs (3, 31). These results explain the decreased amount of transcripts obtained *in vitro* from purified DLPs and provide the basis for the reduced amounts of viral proteins and dsRNAs observed in infected cells treated with ML. Altogether these data indicate that the inhibitor binds VP6, compromising both the integrity of DLPs and the structure of viroplasms.

The mechanism of viroplasm assembly is still not well understood. Viroplasms contain six viral proteins: two non-structural, NSP5 and NSP2 (both shown to be essentially required for viroplasm formation (6, 7, 32)), and four structural proteins, VP1, VP2, VP3 and VP6 (33). Electron microscopy studies suggested that newly made DLPs assemble at the periphery of viroplasms (34). Immunogold labeling of VP6 indicated that this protein localizes exclusively at the periphery of viroplasms, while NSP5, NSP2, and VP2 were also detected in the viroplasm interior (Arnoldi *et al.*, unpublished results). Silencing VP6 expression leads to fewer and smaller viroplasms and reduced amounts of viral mRNAs, viral dsRNAs and viral proteins (5), indicating that this protein is also required for the structural and functional integrity of viroplasms. We confirmed that knocking down VP6 expression produced a sharp reduction in the number of viroplasms (Fig. 8 and (5)), consistently with the capacity of ML to hamper viroplasms by interaction with VP6. However, it is not clear whether the destabilizing

263 effect on viroplasm structure is the consequence of damaging the VP6 layer in newly
264 assembled DLPs or impairing VP6 interactions outside the context of DLPs.

265 Disruption of already assembled viroplasms was particularly evident with OSU and less
266 pronounced with SA11, suggesting that viroplasms may have different stability depending on
267 the strain. The decrease of accumulated viral proteins was nevertheless comparable with the
268 two strains and suggests that ML targets a structural region of VP6 that is conserved among
269 different viruses.

270 Noteworthy, ML did not interfere with formation of VLS nor with recruitment of VP6 into
271 VLS, suggesting that: i) ML does not target the interactions required for VLS assembly (NSP5
272 with either NSP2 or VP2) or for recruitment of VP6 into VLS, that depends on its interaction
273 with VP2 (24); ii) VLS are clearly different from viroplasms, as previously reported (16). The
274 lack of ML effect on VP2-VP6 interaction was further confirmed by the co-immunoprecipitation
275 experiments.

276 Interestingly, a strong reduction of NSP5 hyperphosphorylation was observed upon
277 treatment with ML. NSP5 hyperphosphorylation has been associated to RV replication
278 because of its link with viroplasm formation: i) the two events have been found correlated
279 during the course of viral infection (15); ii) overexpression of NSP5 with either NSP2 or VP2 in
280 uninfected cells induces both NSP5 hyperphosphorylation and VLS formation (13, 24, 25, 35);
281 iii) silencing of casein kinase 1-alpha that affects NSP5 phosphorylation (but does not abolish
282 it entirely) produces viroplasms with irregular shapes (14). Recently, it was shown that at the
283 beginning of infection hypophosphorylated NSP5 interacts with a cytoplasmically dispersed
284 form of NSP2 and was then proposed that during infection phosphorylation of not only NSP5,
285 but also of NSP2, and possibly of VP2, leads to viroplasm maturation (11). Our data in cells
286 treated with both ML and the phosphatase inhibitor okadaic acid show for the first time that

287 NSP5 can remain hyperphosphorylated in infected cells in the absence of viroplasms. Such
288 finding indicates that viroplasms protect NSP5 from dephosphorylation. This result in part
289 supports the model suggested by Criglar *et al.* (11) that proposes an initial interaction among
290 non- or hypophosphorylated viral proteins. However, although a mechanism of concerted
291 phosphorylation involving several proteins of viroplasms might be necessary for subsequent
292 viroplasm maturation and functioning, our data suggest that NSP5 hyperphosphorylation is
293 necessary but not sufficient for viroplasm formation. In this regard, treatment of uninfected
294 cells expressing recombinant NSP5 with inhibitors of cellular phosphatases leads to NSP5
295 hyperphosphorylation, but not to VLS formation (36).

296 So far, a few types of molecules such as proteasome inhibitors (MG132, Bortezomib)
297 (16), MT-depolymerizing drugs (nocodazole, vinblastine) (17), an allosteric inhibitor of Eg5
298 kinesin (monastrol) (17) and thiazolides (18) were shown to affect RV viroplasms.
299 Proteasome inhibitors impair the formation of new viroplasms without affecting the stability of
300 those already assembled, do not show any inhibitory activity on RV particles *in vitro* and do
301 not interfere with the formation of VLS in transfected cells. Although the inhibition mechanism
302 remains obscure, it was hypothesized that the effect was the consequence of blocking
303 proteasome-mediated degradation of an unknown host factor capable of impairing formation
304 of viroplasms (16, 37). Regarding MT-depolymerizing drugs and Eg5 kinesin inhibitor, they
305 both destabilize the viroplasm structure and their coalescence but do not reduce viral proteins
306 expression (17). Finally, treatment with thiazolides causes a reduction in the viroplasm size,
307 resulting in an inhibition of the dsRNA genome segments synthesis, but without impairing viral
308 protein expression or affecting stability of RV particles (18). Importantly, the compound
309 described in this work is the only RV inhibitor so far identified that can disrupt viroplasms and
310 acts on a viral target. This makes the chemical structure of ML particularly appealing for

311 further studies in the field of antivirals. As such, ML could not be used as an antiviral drug,
312 because of its cytotoxicity. However, future research and structural analyses might lead to the
313 development of more potent and selective inhibitors as potential drugs against RV infections.
314
315 **MATERIALS AND METHODS**
316 **Cells and viruses**. MA104 cells (embryonic African green monkey kidney cells, ATCC® CRL-
317 2378) were grown in Dulbecco's Modified Eagle's Medium (DMEM) (Life Technologies)
318 containing 10% Fetal Bovine Serum (Life Technologies), and 50 µg/ml gentamycin (Biochrom
319 AG). BSC-40 cells (green monkey kidney epithelial cells, ATCC® CRL-2761) were cultured in
320 DMEM supplemented with 10% fetal calf serum (AMIMED, Switzerland) and penicillin (100
321 units/ml)-streptomycin (0.1 mg/ml) (Sigma). Sf9 cells (*Spodoptera frugiperda* ovary cells,
322 ATCC® CRL-1711™) were grown in suspension in Sf-900™ II SFM medium (Thermo Fisher
323 Scientific) at 27°C.
324 For RV-infection experiments, the porcine OSU (G5, P9[7]) and simian SA11 4F (G3,
325 P6[1]) strains of RV were used; they were propagated in MA104 cells as described previously
326 (38, 39). Virus titers were determined as described by Eichwald *et al*. (17) and expressed as
327 “viroplasm forming units” (VFU/ml). Purified DLPs were obtained by CsCl gradient purification
328 from infected MA104 cells, essentially as described by Patton *et al*., 2000 (40).
329 For experiments of VLS production and VP6 overexpression in uninfected cells, MA104
330 cells were infected, respectively, with a T7 RNA polymerase recombinant vaccinia virus
331 (strain vvTF7.3) (41), and vvT7/LacOI/VP6 virus (vvVP6), an IPTG-inducible recombinant
332 vaccinia virus driving expression of both the T7 RNA polymerase and VP6 under induction
333 with 1mM IPTG. For generation of vvVP6, BSC-40 cells were infected with recombinant
334 vaccinia virus vvT7/LacOI (42) and transfected with pVOTE.1-VP6. Selection and

amplification were carried out as described by Earl and Moss (43). The plasmid pVOTE.1 and vvT7/LacOI were kindly provided by B. Moss.

For the heterologous production of VP6 protein, the recombinant baculovirus BacVP6C (44) was kindly provided by D. Poncet.

Chemicals. Cells were treated with ML (from 5 to 20 µM, Merck Millipore) following the kinetic indicated in the Results section. Actinomycin D (0.1 µg/ml, Sigma), okadaic acid (0.5 µM, Sigma), and cycloheximide (0.1 µg/ml, Sigma) were added to cells from 3 to 8 hours post-infection (hpi). Purified DLPs were treated with ML (from 2.5 to 200 µM, as indicated in the Results section) or with 200 µM of irrelevant compound (ID #7749832, ChemBridge Corp).

Plasmid constructions. The plasmids pcDNA3-NSP5, -NSP2, -VP6 and -VP2 used to overexpress RV proteins in uninfected cells were already described previously (13, 35, 45). The plasmid pVOTE.1-VP6 was obtained by PCR amplification of VP6 mouse EC strain, using specific primers (5'-ATGCCCATGGATGTGCTGTACTCCATC-3' and 5'-GATCGGATCCTCACTT TACCAGCATGCTTCT-3') to incorporate NcoI and BamHI restriction sites at the 5' and 3' ends, respectively. The amplified fragment was ligated between NcoI and BamHI restriction sites in pVOTE.1 (42). All primer sequences used in this study for PCR and sequencing are available upon request to the authors.

Infections and transient transfections. Infection experiments with RV were carried out at an MOI of 25 VFU/cell (17). For overexpression of RV proteins in uninfected cells, confluent monolayers of MA104 cells in 12-well plates were infected with vvTF7.3 at an MOI of 10 pfu/cell (41, 46). At 1 hpi, cells were transfected with a total of 2 µg of DNA plasmid using Lipofectamine 3000 (ThermoFisher Scientific) according to the manufacturer's instructions. At 16 hpi, cells were washed once to remove serum and then treated with 10 µM ML in serum-free DMEM medium for 5 hours. Cells were then collected for immunofluorescence or

359 Western blot analyses. For VP6 overexpression, confluent monolayers of MA104 cells in 12-
360 well plates were infected with vvVP6 (MOI; 10 pfu/cell). At 1 hpi, both 1mM IPTG and 10 µM
361 ML were added, and 7 h later cells were collected for immunofluorescence or Western blot
362 analyses.

363 For experiments with siRNAs against VP6 (siVP6-OSU:
364 UGGAACCAUCAUAGCUAGAAA; siVP6-SA11: UGGAACUAUCGUAGCUAGAAA), $5x10^4$
365 MA104 cells per well were seeded into 12-well plates and the next day transfected with 0.1
366 nmol of annealed duplex siRNA (Sigma) using 5 µl of RNAiMAX Lipofectamine 2000
367 (ThermoFisher Scientific) according to the manufacturer's instructions. Control siRNAs were
368 siNSP5-SA11 and siNSP5-OSU here referred as siNT and described by Campagna *et al.*,
369 2005 (7). At 48 hpt cells were infected at the same MOI and collected at 6 hpi (for viroplasm
370 counting by immunofluorescence or Western blot analyses).

371 Cellular extracts (about 3 x 10^5 cells) were prepared with 50 µl of reducing SDS buffer
372 (125 mM Tris-HCl pH 6.8, 6% SDS, 40% glycerol, 5% β-mercaptoethanol, 0.04%
373 bromophenol blue) and subsequently sonicated with a VialTweeter (Hielscher Ultrasonics
374 GmbH) for 1 min (10 W, pulse 0.5 sec) to disrupt DNA. Typically, 10 µl of cellular extracts
375 were loaded onto an SDS-polyacrylamide gel for Western blot analyses. For VP6 trimer
376 analyses, cellular extracts were prepared in TNN lysis buffer (100 mM Tris-HCl, pH 8, 250
377 mM NaCl, 0.5% NP-40 and 30 mM *N*-ethylmaleimide) and centrifuged at 5,000 x g for 5 min
378 at 4˚C. For immunoprecipitation assays, cellular extracts were prepared in
379 radioimmunoprecipitation assay (RIPA) buffer (10 mM Tris-HCl, 1% Triton X-100, 0.5%
380 sodium deoxycholate, 1 mM EDTA, 150 mM NaCl [pH 7.4]), incubated on ice for 15 min, and
381 then centrifuged at 13,000 x g for 5 min at 4˚C.

382 **Immunoprecipitation and protein analysis.** For immunoprecipitation assays, usually 4/5 of
383 the total extract, i.e. approximately 80 µl, were immunoprecipitated for 2h at 4°C after addition
384 of 100 µl of an undiluted mouse anti-VP6 (clone RV138) monoclonal antibody supernatant
385 (47) (kindly provided by D. Agnello and P. Pothier), 1 µl of a Protease Inhibitor Cocktail
386 (Sigma), and 50 µl of 50% immobilised rProtein A beads (Repligen Bioprocessing) in RIPA
387 buffer. Beads were washed four times with RIPA buffer, followed by one wash with PBS and
388 resuspended in 20 µl of loading buffer. Proteins were separated by SDS-polyacrylamide gel
389 and transferred to polyvinylidene difluoride membranes (Millipore, IPVH00010) (48). For
390 protein analysis of either cellular extracts or immunoprecipitated proteins, membranes were
391 incubated with the following primary antibodies: anti-NSP5 (1:10,000) (46), anti-VP2 (1:5,000)
392 (35), anti-RV (1:2,500) (17), anti-VP1 (1:5,000) (35) guinea pig sera, anti-NSP3 rabbit serum
393 (1:1,500) (kindly provided by S. López), anti-NSP4 rabbit serum (1:1,1000) (kindly provided
394 by D. Luque), anti-VP5 clone 2G4 mouse monoclonal antibody (1:2,000) (kindly provided by
395 H. Greenberg), anti-alpha-tubulin mouse monoclonal antibody (1:3,000, Calbiochem), anti-
396 actin rabbit polyclonal antibody (1:1,000, Sigma). The membranes were then incubated with
397 the corresponding HRP-conjugated goat anti-guinea pig (1:10,000, Jackson
398 ImmunoResearch), goat anti-mouse (1:5,000, Jackson ImmunoResearch), goat anti-rabbit
399 (1:5,000, Thermo Scientific Pierce) secondary antibodies. Signals were detected by using the
400 enhanced chemiluminescence system (Pierce ECL Western Blotting Substrate, Thermo
401 Scientific).

402 **Immunofluorescence microscopy.** Immunofluorescence experiments were performed as
403 described previously (49) using the following antibody dilutions: anti-NSP5 guinea pig serum
404 1:1,000; anti-VP6 mouse monoclonal antibody (clone 4B2D2) 1:1,000 (kindly provided by J. L.
405 Zambrano and F. Liprandi); Alexa Fluor® 488-conjugated anti-mouse (1:500, Life

406 Technologies) and Alexa Fluor® 546-conjugated anti-rabbit (1:500, Life Technologies)
407 secondary antibodies. Newly synthesized RNAs were labeled using 2 mM ethylene uridine
408 (EU) ribonucleotide homolog containing an alkyne reactive group, and the modified
409 incorporated nucleotide was revealed with an azide-containing fluorophore (Alexa-488,
410 green), as described for Click-iT® RNA Alexa Fluor® 488 Imaging Kit (Thermo Fisher
411 Scientific). Cell nuclei were stained with 2 µg/ml Hoechst 33342 (Molecular Probes, Life
412 Technologies). Samples were analyzed by confocal microscopy (Zeiss LSM510 equipped
413 with a 100x NA 1.3 objective), and images were processed using LSM Image Examiner 4.0
414 Software.
415 **Analysis of RV genome segments.** Total RNA was purified from MA104 cells infected with
416 OSU (MOI; 25 VFU/cell) after treatment with 10 µM ML or a control vehicle (dimethyl
417 sulfoxide, DMSO) from 1 to 6 hpi. Crude viral preparations were digested with 10 µg/ml of
418 proteinase K (Thermo Fisher Scientific) in the presence of 5 mM EDTA and 0.5% SDS, for 30
419 min at 60°C. RNA was then purified by phenol-chloroform extraction and precipitation with 5M
420 ammonium acetate and quantified using the NanoDrop 1000 Spectrophotometer (Thermo
421 Fisher Scientific). 3.5 µg of total RNA were separated by Tris-glycine nondenaturing
422 polyacrylamide (4% stacking gel, 10% resolving gel) and transferred to a charged nylon
423 membrane (GeneScreen Plus Hybridization Transfer Membrane, Perkin Elmer). The
424 membrane was blocked with 5% milk and 50 µg/ml DNA fish sperm (Affymetrix) in PBS and
425 was incubated overnight with the mouse anti-dsRNA (clone J2) monoclonal antibody (1:1,000;
426 English and Scientific Consulting Bt., Hungary) (50), followed by reaction with HRP-
427 conjugated goat anti-mouse antibody (1:5,000, Jackson ImmunoResearch).
428 **Cell viability assay**. $2x10^5$ MA104 cells were seeded in 12-well plates. After infection and
429 drug treatment for the indicated time points, supernatants were removed and stored and cells

were trypsinized (0.5% trypsin-EDTA, Gibco, ThermoFisher Scientific) and then mixed with supernatants in order not to lose suffering cells possibly detached. After centrifugation at 900 x g for 2 min at room temperature (RT), pellets were resuspended in 200 µl of 0.5 ng/µl propidium iodide in PBS and incubated in the dark for 15 min at RT. Samples were diluted to 1 ml with PBS, filtered using a cell strained snap-cap tube (BD Falcon™) and immediately acquired in a Gallios™ Flow Cytometer (Beckman Coulter, Inc.). For this purpose, 10,000 events were acquired, exciting at 488 nm with an argon laser and a filter band of 675/20 BP. Data were analyzed gating on live cells using a Kaluza® Flow Analysis Software. The statistical analysis and plot were performed using Microsoft® Excel® for MAC 2011 Version 14.7.0.

Determination of progeny virus yield. $2x10^5$ MA104 cells seeded in 12-well plates were RV-infected with an MOI of 25 VFU/cell. Virus adsorption was performed for 1 h at 4˚C, followed by incubation at 37˚C. At 2 hpi, cells were washed twice with PBS and 10µM ML or vehicle (2% DMSO) diluted in 500µl DMEM was added. At the indicated time points, plates were frozen at -80˚C. Cells were then treated with three freeze-thaw cycles, harvested and centrifuged at 17,000 x g for 5 min at 4˚C. The supernatant was recovered and activated with 80µg/ml of trypsin for 30 min at 37˚C. Serial dilutions were prepared and used to determine the viral titers as described by Eichwald *et al*., 2012 (17).

***In vitro* transcription assays with purified DLPs.** 1 µg of purified DLPs were incubated for 4 h at 42°C in a total volume of 100 µl of 1X T7 transcription buffer from Promega, 2mM of each NTP, 0.5 mM SAM, 0.1 mM $MnCl_2$, 1mM DTT, 0.4 U RNAsin® (Promega). RNA was isolated using the GeneJET RNA Cleanup and concentration Micro kit (Thermo Fisher Scientific) and quantified using the Qubit RNA Assay Kits associated to a Qubit 2.0

453 Fluorometer (Thermo Fisher Scientific). The statistical analyses were performed using
454 Student's t-Test by comparing vehicle and ML-treated particles of each viral strain.
455 **Production of recombinant Baculovirus VP6.** A Sf9 suspension culture (1 x 10^6 cells/ml)
456 was infected with recombinant baculovirus BacVP6C (27). At 3 days post-infection, cells were
457 harvested by centrifugation at 180 x g for 20 min at 4°C. The cellular pellet was resuspended
458 in 10 ml of 20 mM MOPS buffer (pH 6.8) followed by dilution in one volume of
459 trichlorofluoromethane (Sigma). The sample was vortexed for 1 min and centrifuged at 4,500
460 x g for 5 min at 4°C. The aqueous phase was transferred to a new tube and this step
461 repeated twice. The sample was then ultracentrifuged at 100,000 x g with a Beckman SW70.2
462 rotor for 3 h at 4˚C. The pellet was resuspended in 3 ml of 50 mM Tris-HCl, pH 8.0, 150 mM
463 $CaCl_2$, 200 mM NaCl to promote formation of VP6 isolated trimers. Trimeric VP6 was further
464 purified by size exclusion chromatography (Superdex200 16/60 equipped on an AKTA
465 system) and stored at 4 °C.
466 **Transmission electron microscopy.** For detection of viroplasms, MA104 cells were seeded
467 at 1x10^5 cells in a 2 cm^2 well onto sapphire discs and infected with OSU [MOI: 100 VFU/cell]
468 (17). At 1 hpi, 20 µM ML was added. At 6 hpi, cells were fixed with 2.5% glutaraldehyde in
469 100 mM Na/K-phosphate buffer, pH 7.4 for 1 h at 4˚C and kept in 100 mM Na/K-phosphate
470 buffer overnight at 4˚C. Afterwards, samples were post-fixed in 1% osmium tetroxide in 100
471 mM Na/K-phosphate buffer for 1 h at 4˚C, dehydrated in a graded ethanol series starting at
472 70% followed by two changes in acetone and embedded in epon. Ultrathin sections (60-80
473 nm) were cut, stained with uranyl acetate and lead citrate. For EM analyses of purified DLPs
474 incubated with ML for 4 h at 42˚C (in the same buffer used in *in vitro* transcription assays),
475 DLPs were adsorbed for 10 min on glow-discharged carbon-coated Parlodion films mounted
476 on 300 mesh per inch copper grids (EMS). Samples were washed once with distilled water

and stained with saturated uranyl acetate (Fluka) for 1 min at RT. Samples were analyzed in a transmission electron microscope (CM12, Philips, Eindhoven, The Netherlands) equipped with a CCD camera (Ultrascan 1000, Gatan, Pleasanton, CA, USA) at an acceleration of 100 kV. For negative staining EM experiments of purified VP6, aliquots of trimeric VP6 (0.5 mg/ml) were dialyzed overnight at 4˚C against either 50 mM MOPS, pH 6.0, 50 mM NaCl or 50 mM sodium acetate, pH 4.0 to reconstitute VP6 nanotubes and spheres, respectively. After dialysis, VP6 samples were recovered and incubated in the presence or absence of 25 µM ML for 4 h at 37˚C (1% DMSO in both conditions). Prior to sample application, the 400-mesh copper carbon-coated grids (Agar Scientific) were glow-discharged for 30 sec at 30 mA using a GloQube system (Quorum Technologies). A 4-µl drop of the incubated VP6 samples at a final concentration of 0.25 mg/ml was applied to the glow-discharged grid and incubated for 1 min. The grid was immediately stained by gentle stirring for 1 min using 2% (w/v) uranyl acetate solution. After staining, the grid was blotted dry and imaged on a Tecnai G2 T20 LaB6 transmission electron microscope (FEI) operating at 200 KeV. Images were manually acquired on an Eagle 2K CCD camera (FEI) at a nominal magnification of 50,000× (corresponding to a pixel size of 4.55 Å at the specimen level) and defocus values in the range of 1.5 µm to 2.5 µm.

Microscale thermophoresis. Thermophoresis was used to determine the binding affinities between recombinant purified VP6 and ML. Experiments were performed in standard capillaries using a Monolith™ NT.115 instrument (NanoTemper Technologies). Either cysteines or lysines of VP6 were labeled with maleimide or NHS dye, respectively, following the manufacturer protocol. Labeled VP6 (100 nM) was incubated at 37 °C for 4 h with increasing concentration of ML (0 to 10^6 nM) in MST buffer (50 mM Tris-HCl, pH 7.4, 150 mM NaCl, 10 mM MgCl2, 0.05% Tween-20) supplemented with 10% DMSO. Thereafter,

measurements were performed at 24 °C using 20% LED power and 20% MST power. The addition of ML causes quenching of the fluorescent protein due to specific binding, as assessed by the SD-test; therefore, initial fluorescence was used to calculate the affinity. Data were analyzed according to the Hill model (cooperative binding) using the NanoTemper software. Reported affinity value is the average of three independent experiments.

ACKNOWLEDGMENTS

We are grateful to Didier Poncet (Institut de Biologie Intégrative de la Cellule, UMR CNRS, CEA, Univ. PARIS XI, Paris, France) for providing us with BacVP6C; to Bernard Moss (National Institutes of Health, Bethesda, MD, USA) for the pVOTE.1 plasmid and the vvT7/LacOI virus; to Davide Agnello and Pierre Pothier (CNR des virus des gastroentérites, CHU de Dijon, Dijon, France) for the mouse anti-VP6 (clone RV138) monoclonal antibody, and to Jose Luis Zambrano and Ferdinando Liprandi (Instituto Venezolano de Investigaciones Científicas, Caracas, Venezuela) for providing us with the mouse anti-VP6 (clone 4B2D2) monoclonal antibody; to Susana López (Instituto de Biotecnología, UNAM, Cuernavaca, Mexico) for the rabbit anti-NSP3 antibody; to Daniel Luque (Centro Nacional de Microbiología, ISCIII, Madrid, Spain) for the rabbit anti-NSP4 antibody and to Harry Greenberg (Stanford University, CA, USA) for the mouse anti-VP5 monoclonal antibody (clone 2G4). We would like to thank Peter Wild for his advice and critical reading.

Most experiments of this study and the work by FA and MB were supported by a FIRB-Futuro in Ricerca grant (RBFR13209E) funded by the Ministero dell'Istruzione, dell'Università e della Ricerca (MIUR), Italy. Also, this work was supported by a private donation of the late Prof Dr. Robert Wyler to MA (F-52601-10-01) as well as by general funds allocated to MA by the University of Zurich. GDL and GP were supported by an ICGEB pre-doctoral fellowship.

The work by MDR, EM, and MM was supported by PRIN 2012 NOXSS (X-ray Single Shots of Nano-Objects), MIUR prot. 2012Z3N9R9.

REFERENCES

1. Tate JE, Burton AH, Boschi-Pinto C, Parashar UD, World Health Organization-Coordinated Global Rotavirus Surveillance N. 2016. Global, regional, and national estimates of rotavirus mortality in children <5 years of age, 2000-2013. Clin Infect Dis 62 Suppl 2:S96-S105.
2. Desselberger U. 2014. Rotaviruses. Virus Res 190:75-96.
3. Bican P, Cohen J, Charpilienne A, Scherrer R. 1982. Purification and characterization of bovine rotavirus cores. J Virol 43:1113-1117.
4. Kohli E, Pothier P, Tosser G, Cohen J, Sandino AM, Spencer E. 1993. *In vitro* reconstitution of rotavirus transcriptional activity using viral cores and recombinant baculovirus expressed VP6. Arch Virol 133:451-458.
5. Ayala-Breton C, Arias M, Espinosa R, Romero P, Arias CF, Lopez S. 2009. Analysis of the kinetics of transcription and replication of the rotavirus genome by RNA interference. J Virol 83:8819-8831.
6. Lopez T, Rojas M, Ayala-Breton C, Lopez S, Arias CF. 2005. Reduced expression of the rotavirus NSP5 gene has a pleiotropic effect on virus replication. J Gen Virol 86:1609-1617.
7. Campagna M, Eichwald C, Vascotto F, Burrone OR. 2005. RNA interference of rotavirus segment 11 mRNA reveals the essential role of NSP5 in the virus replicative cycle. J Gen Virol 86:1481-1487.

548 8. Patton JT, Silvestri LS, Tortorici MA, Vasquez-Del Carpio R, Taraporewala ZF. 2006.
549 Rotavirus genome replication and morphogenesis: role of the viroplasm. Curr Top
550 Microbiol Immunol 309:169-187.
551 9. Vascotto F, Campagna M, Visintin M, Cattaneo A, Burrone OR. 2004. Effects of
552 intrabodies specific for rotavirus NSP5 during the virus replicative cycle. J Gen Virol
553 85:3285-3290.
554 10. Afrikanova I, Miozzo MC, Giambiagi S, Burrone O. 1996. Phosphorylation generates
555 different forms of rotavirus NSP5. J Gen Virol 77 (Pt 9):2059-2065.
556 11. Criglar JM, Hu L, Crawford SE, Hyser JM, Broughman JR, Prasad BV, Estes MK.
557 2014. A novel form of rotavirus NSP2 and phosphorylation-dependent NSP2-NSP5
558 interactions are associated with viroplasm assembly. J Virol 88:786-798.
559 12. Poncet D, Aponte C, Cohen J. 1996. Structure and function of rotavirus nonstructural
560 protein NSP3. Arch Virol Suppl 12:29-35.
561 13. Afrikanova I, Fabbretti E, Miozzo MC, Burrone OR. 1998. Rotavirus NSP5
562 phosphorylation is up-regulated by interaction with NSP2. J Gen Virol 79 (Pt 11):2679-
563 2686.
564 14. Campagna M, Budini M, Arnoldi F, Desselberger U, Allende JE, Burrone OR. 2007.
565 Impaired hyperphosphorylation of rotavirus NSP5 in cells depleted of casein kinase
566 1alpha is associated with the formation of viroplasms with altered morphology and a
567 moderate decrease in virus replication. J Gen Virol 88:2800-2810.
568 15. Poncet D, Lindenbaum P, L'Haridon R, Cohen J. 1997. *In vivo* and *in vitro*
569 phosphorylation of rotavirus NSP5 correlates with its localization in viroplasms. J Virol
570 71:34-41.

16. Contin R, Arnoldi F, Mano M, Burrone OR. 2011. Rotavirus replication requires a functional proteasome for effective assembly of viroplasms. Journal of Virology 85:2781-2792.

17. Eichwald C, Arnoldi F, Laimbacher AS, Schraner EM, Fraefel C, Wild P, Burrone OR, Ackermann M. 2012. Rotavirus viroplasm fusion and perinuclear localization are dynamic processes requiring stabilized microtubules. PLoS One 7:e47947.

18. La Frazia S, Ciucci A, Arnoldi F, Coira M, Gianferretti P, Angelini M, Belardo G, Burrone OR, Rossignol JF, Santoro MG. 2013. Thiazolides, a new class of antiviral agents effective against rotavirus infection, target viral morphogenesis, inhibiting viroplasm formation. J Virol 87:11096-11106.

19. Smee DF, Sidwell RW, Clark SM, Barnett BB, Spendlove RS. 1982. Inhibition of rotaviruses by selected antiviral substances: mechanisms of viral inhibition and *in vivo* activity. Antimicrob Agents Chemother 21:66-73.

20. Wu L, Pan J, Thoroddsen V, Wysong DR, Blackman RK, Bulawa CE, Gould AE, Ocain TD, Dick LR, Errada P, Dorr PK, Parkinson T, Wood T, Kornitzer D, Weissman Z, Willis IM, McGovern K. 2003. Novel small-molecule inhibitors of RNA polymerase III. Eukaryot Cell 2:256-264.

21. Perry RP, Kelley DE. 1970. Inhibition of RNA synthesis by actinomycin D: characteristic dose-response of different RNA species. J Cell Physiol 76:127-139.

22. Song W, Filonov GS, Kim H, Hirsch M, Li X, Moon JD, Jaffrey SR. 2017. Imaging RNA polymerase III transcription using a photostable RNA-fluorophore complex. Nat Chem Biol 13:1187-1194.

593 23. Sabara M, Ready KF, Frenchick PJ, Babiuk LA. 1987. Biochemical evidence for the
594 oligomeric arrangement of bovine rotavirus nucleocapsid protein and its possible
595 significance in the immunogenicity of this protein. J Gen Virol 68 (Pt 1):123-133.
596 24. Contin R, Arnoldi F, Campagna M, Burrone OR. 2010. Rotavirus NSP5 orchestrates
597 recruitment of viroplasmic proteins. J Gen Virol 91:1782-1793.
598 25. Fabbretti E, Afrikanova I, Vascotto F, Burrone OR. 1999. Two non-structural rotavirus
599 proteins, NSP2 and NSP5, form viroplasm-like structures *in vivo*. J Gen Virol 80 (Pt
600 2):333-339.
601 26. Lepault J, Petitpas I, Erk I, Navaza J, Bigot D, Dona M, Vachette P, Cohen J, Rey FA.
602 2001. Structural polymorphism of the major capsid protein of rotavirus. Embo J
603 20:1498-1507.
604 27. Petitpas I, Lepault J, Vachette P, Charpilienne A, Mathieu M, Kohli E, Pothier P, Cohen
605 J, Rey FA. 1998. Crystallization and preliminary X-Ray analysis of rotavirus protein
606 VP6. J Virol 72:7615-7619.
607 28. Ablasser A, Bauernfeind F, Hartmann G, Latz E, Fitzgerald KA, Hornung V. 2009. RIG-
608 I-dependent sensing of poly(dA:dT) through the induction of an RNA polymerase III-
609 transcribed RNA intermediate. Nat Immunol 10:1065-1072.
610 29. Chiu YH, Macmillan JB, Chen ZJ. 2009. RNA polymerase III detects cytosolic DNA and
611 induces type I interferons through the RIG-I pathway. Cell 138:576-591.
612 30. Karijolich J, Abernathy E, Glaunsinger BA. 2015. Infection-induced retrotransposon-
613 derived noncoding RNAs enhance herpesviral gene expression via the NF-kappaB
614 pathway. PLoS Pathog 11:e1005260.

615 31. Charpilienne A, Lepault J, Rey F, Cohen J. 2002. Identification of rotavirus VP6
616 residues located at the interface with VP2 that are essential for capsid assembly and
617 transcriptase activity. J Virol 76:7822-7831.
618 32. Silvestri LS, Taraporewala ZF, Patton JT. 2004. Rotavirus replication: plus-sense
619 templates for double-stranded RNA synthesis are made in viroplasms. J Virol 78:7763-
620 7774.
621 33. Petrie BL, Greenberg HB, Graham DY, Estes MK. 1984. Ultrastructural localization of
622 rotavirus antigens using colloidal gold. Virus Res 1:133-152.
623 34. Cuadras MA, Bordier BB, Zambrano JL, Ludert JE, Greenberg HB. 2006. Dissecting
624 rotavirus particle-raft interaction with small interfering RNAs: insights into rotavirus
625 transit through the secretory pathway. J Virol 80:3935-3946.
626 35. Arnoldi F, Campagna M, Eichwald C, Desselberger U, Burrone OR. 2007. Interaction
627 of rotavirus polymerase VP1 with nonstructural protein NSP5 is stronger than that with
628 NSP2. J Virol 81:2128-2137.
629 36. Blackhall J, Munoz M, Fuentes A, Magnusson G. 1998. Analysis of rotavirus
630 nonstructural protein NSP5 phosphorylation. J Virol 72:6398-6405.
631 37. Lopez T, Silva-Ayala D, Lopez S, Arias CF. 2011. Replication of the rotavirus genome
632 requires an active ubiquitin-proteasome system. J Virol 85:11964-11971.
633 38. Estes MK, Graham DY, Gerba CP, Smith EM. 1979. Simian rotavirus SA11 replication
634 in cell cultures. J Virol 31:810-815.
635 39. Graham A, Kudesia G, Allen AM, Desselberger U. 1987. Reassortment of human
636 rotavirus possessing genome rearrangements with bovine rotavirus: evidence for host
637 cell selection. J Gen Virol 68 (Pt 1):115-122.

638 40. Patton J, Chizhikov V, Taraporewala Z, Chen DY. 2000. Virus replication, p 33-66. *In*
639 Gray J, Desselberger U (ed), Rotaviruses methods and Protocols. Humana Press,
640 Totowa, New Jersey.
641 41. Fuerst TR, Moss B. 1989. Structure and stability of mRNA synthesized by vaccinia
642 virus-encoded bacteriophage T7 RNA polymerase in mammalian cells. Importance of
643 the 5' untranslated leader. J Mol Biol 206:333-348.
644 42. Ward GA, Stover CK, Moss B, Fuerst TR. 1995. Stringent chemical and thermal
645 regulation of recombinant gene expression by vaccinia virus vectors in mammalian
646 cells. Proc Natl Acad Sci U S A 92:6773-6777.
647 43. Earl PL, Moss B, Wyatt LS, Carroll MW. 2001. Generation of recombinant vaccinia
648 viruses. Curr Protoc Mol Biol Chapter 16:Unit16 17.
649 44. Tosser G, Labbe M, Bremont M, Cohen J. 1992. Expression of the major capsid
650 protein VP6 of group C rotavirus and synthesis of chimeric single-shelled particles by
651 using recombinant baculoviruses. J Virol 66:5825-5831.
652 45. De Lorenzo G, Eichwald C, Schraner EM, Nicolin V, Bortul R, Mano M, Burrone OR,
653 Arnoldi F. 2012. Production of *in vivo*-biotinylated rotavirus particles. J Gen Virol
654 93:1474-1482.
655 46. Gonzalez SA, Burrone OR. 1991. Rotavirus NS26 is modified by addition of single O-
656 linked residues of N-acetylglucosamine. Virology 182:8-16.
657 47. Kohli E, Maurice L, Vautherot JF, Bourgeois C, Bour JB, Cohen J, Pothier P. 1992.
658 Localization of group-specific epitopes on the major capsid protein of group A
659 rotavirus. J Gen Virol 73 (Pt 4):907-914.
660 48. Eichwald C, Jacob G, Muszynski B, Allende JE, Burrone OR. 2004. Uncoupling
661 substrate and activation functions of rotavirus NSP5: phosphorylation of Ser-67 by

casein kinase 1 is essential for hyperphosphorylation. Proc Natl Acad Sci U S A 101:16304-16309.

49. Eichwald C, Vascotto F, Fabbretti E, Burrone OR. 2002. Rotavirus NSP5: mapping phosphorylation sites and kinase activation and viroplasm localization domains. J Virol 76:3461-3470.

50. DeWitte-Orr SJ, Mehta DR, Collins SE, Suthar MS, Gale M, Jr., Mossman KL. 2009. Long double-stranded RNA induces an antiviral response independent of IFN regulatory factor 3, IFN-beta promoter stimulator 1, and IFN. J Immunol 183:6545-6553.

FiGURE LEGENDS

Fig. 1. ML effect on RV replication. (A-E) Western blot and confocal immunofluorescence analysis with the indicated antibodies of RV-infected cells (MOI, 25 VFU/cell) treated with ML at 10 µM, unless otherwise indicated, or DMSO (D) for the indicated time windows. Scale bars, 10 µm. (F) Time course of viral progeny yield of OSU-infected (MOI, 25 VFU/cell) MA104 cells treated with 10 µM ML, added at 2 hpi. Data are presented as average ± standard deviation of three independent experiments. t-Test, (***) $p<0.001$. (G) Genome segments analysis of blotted total RNA extracted from non-infected (NI) and OSU-infected MA104 cells (25 VFU/cell) treated with ML (10 µM) or DMSO from 1 to 8 hpi and revealed with an anti-dsRNA antibody. (H) Viability of non-infected or OSU-infected (MOI, 25 VFU/cell) MA104 cells determined by cytofluorometry of propidium iodide stained cells following treatment at 2 hpi with or without 10 µM ML for up to 12 hpi. Data are presented as average ± standard deviation of three independent experiments. T-test, (*)$p<0.05$; (**) $p<0.01$ and (***) $p<0.001$.

686 **Fig. 2. Electron microscopy of RV-infected cells treated with ML.** High-definition electron
687 microscopy of non-infected (NI) and RV-infected (OSU; MOI, 100 VFU/ml) MA104 cells
688 untreated (DMSO) or treated with ML (20 μM) from 1 hpi. At 6 hpi, cells were fixed with
689 glutaraldehyde and processed for transmission electron microscopy. V, viroplasms; Nu,
690 nucleus, ER, endoplasmic reticulum; Gg, Golgi complex; Vc, vacuoles; P_h, phagosomes; CM,
691 cell membrane; thin white arrows indicate the endoplasmic reticulum membrane surrounding
692 viroplasms; solid white arrowheads indicate viral particles. The corresponding scale bars are
693 shown in each image.
694 **Fig. 3. NSP5 dephosphorylation caused by ML-mediated viroplasm disruption.** Western
695 blot and confocal immunofluorescence analysis with the indicated antibodies of OSU-infected
696 MA104 cells (25 VFU/cell) treated with 10 μM ML and/or 0.5 μM okadaic acid (OA) or DMSO
697 for the indicated time windows. Scale bars, 5 μm.
698 **Fig. 4. ML antiviral activity is independent of cellular transcription and protein**
699 **synthesis.** (A) Western blot and confocal immunofluorescence analysis with the indicated
700 antibodies of OSU-infected MA104 cells (25 VFU/cell) fed with ethynyl uridine (EU) and
701 treated with 10 μM ML and/or 10 μg/ml actinomycin D or DMSO for the indicated time
702 windows. EU-labeled, newly synthesized RNAs were visualized by reaction with an Alexa-488
703 conjugated azide (green). Scale bars, 5 μm. (B) Western blot and confocal
704 immunofluorescence with the indicated antibodies of OSU-infected (MOI, 25 VFU/cell) MA104
705 cells treated with 10 μM ML and/or 10 μg/ml cycloheximide (CHX) or DMSO for the indicated
706 time windows. Scale bars, 10 μm.
707 **Fig. 5. ML-mediated impairment of DLP stability.** (A) Transcriptional activity of purified
708 DLPs. The plot shows the dose-dependent decrease of transcripts produced by SA11 or OSU
709 DLPs incubated in the presence of the indicated concentrations of ML. The small molecule ID

#7749832 (ChemBridge Corp.) at 200 μM was used as an irrelevant compound (irr.). The data represent the mean ± standard deviation of at least three independent experiments. t-Test, (**)p<0.01, (***)p<0.001 and ns, p>0.01. (B-C) DLPs morphology analyzed by electron microscopy. Purified DLPs were incubated for 4 h with the indicated concentrations of ML or DMSO. Open white arrows indicate damaged DLPs with an irregular shape and partially open. Quantification of damaged DLPs is shown in C. The data in graph C are presented as average ± SEM; t-test (***) p<0.001; n>100.

Fig. 6. Effect of ML on RV VP6. (A) VP6-VP2 interaction. Western blot analysis with anti-VP2 and anti-VP6 antibodies of immunoprecipitates (IP) obtained with anti-VP6 mAb RV138 from extracts of MA104 cells transfected with VP6 and VP2 and treated for 5 h with 10 μM ML or DMSO. The inhibitor (200 μM) was maintained during cell lysis and incubation with the precipitating antibody. (B) VP6 trimer stability. Left panel: Western blot analysis with anti-VP6 antibody of non-boiled extracts from MA104 cells infected with a recombinant vaccinia virus expressing VP6 (vvVP6) and treated with 10 μM ML or DMSO from 1 to 7 hpi. Right panel: Western blot analysis of non-boiled extracts from cells infected with OSU (MOI, 25 VFU/cell) treated with 10 μM ML or DMSO from 1 to 5 hpi. (C) Confocal immunofluorescence analysis with the anti-VP6 mAb 4B2D2 of MA104 cells overexpressing VP6 (infected with vvVP6) and treated with 10 μM ML or DMSO from 1 to 7 hpi. The white arrow indicates a VP6 higher order structure observed in the absence of other RV proteins. Scale bars, 5 μm. (D) Representative images of VP6 tubes and spheres visualized by negative staining electron microscopy after treatment with 25 μM ML for 4 h at 37˚C. Scale bar, 100 nm. (E) Interaction of VP6 with ML evaluated by nanoscale thermophoresis. The fraction of Cys- or Lys-labeled VP6 bound to ML was plotted against increasing concentrations of the inhibitor. Data were

fitted with two state equations and an EC_{50} of 294 ± 62 µM calculated as the average of three independent measurements.

Fig. 7. ML effect on VLS. Confocal immunofluorescence of VLS (A, C) and Western blot analysis (B) with the indicated antibodies of MA104 cells transfected with NSP5, NSP2, VP2 and VP6, as indicated. In (A) NSP5 is shown in green and NSP2 or VP2 in red. In (C) NSP5 is shown in red, and VP6 in green. Cells were treated for 5 h with 10 µM ML or DMSO at 18 h post-transfection.

Fig. 8. VP6 in RV-infected cells. Confocal immunofluorescence of MA104 cells infected with either OSU or SA11 (MOI, 25 VFU/cell) and: A) transfected with siRNAs specific for SA11 VP6 or OSU VP6, or with a non-targeting siRNA (siNT); B) treated with 10 µM ML or DMSO. At the times points post-infection indicated viroplasms were visualized with anti-NSP5 antibody (red) and VP6 with mAb 4B2D2 (green). Scale bars, 5 µm.

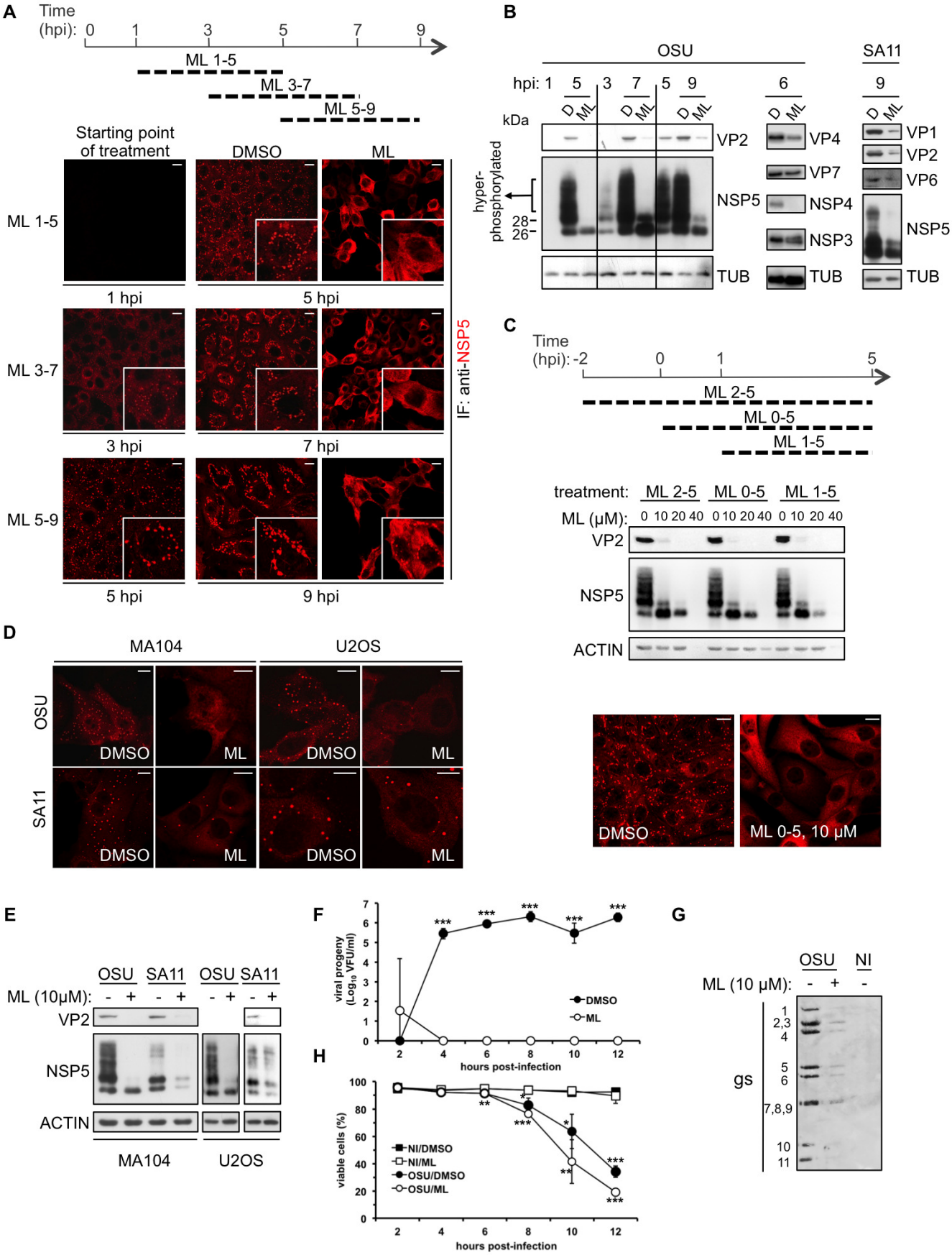

Journal of Virology

JVI

Journal of Virology